Change in Electronic Structure upon Optical Excitation of 8-Vinyladenosine: An Experimental and Theoretical Study

ARTICLE *in* THE JOURNAL OF PHYSICAL CHEMISTRY A · NOVEMBER 2009

Impact Factor: 2.69 · DOI: 10.1021/jp908055h · Source: PubMed

Change in Electronic Structure upon Optical Excitation of 8-Vinyladenosine: An Experimental and Theoretical Study

Goutham Kodali, Kurt A. Kistler, Madhavan Narayanan, Spiridoula Matsika, and Robert J. Stanley*

Department of Chemistry, Temple University, Philadelphia, Pennsylvania 19122

Received: August 20, 2009; Revised Manuscript Received: September 30, 2009

8-Vinyladenosine (8VA) is an adenosine analog, like 2-aminopurine (2AP), that has a red-shifted absorption and high fluorescence quantum yield. When introduced into double-stranded DNA (dsDNA), its base-pairing and base-stacking properties are similar to those of adenine. Of particular interest, the fluorescence quantum yield of 8VA is sensitive to base stacking, making it a very useful real-time probe of DNA structure. The fundamental photophysics underlying this fluorescence quenching by base stacking is not well understood, and thus exploring the excited state electronic structure of the analog is warranted. In this study, we report on changes in the electronic structure of 8VA upon optical excitation. Stark spectroscopy was performed on 8VA monomer in frozen ethanol glass at 77 K to obtain the direction and degree of charge redistribution in the form of the difference dipole moment, $\Delta\vec{\mu}_{01} = 4.7 \pm 0.3$ D, and difference static polarizability, $\mathrm{tr}(\Delta\vec{\vec{\alpha}}_{01}) = 21 \pm 11$ Å^3, for the $S_0 \rightarrow S_1$ transition. In addition, solvatochromism experiments were performed on 8VA in various solvents and analyzed using Bakhshiev's model. High level ab initio methods were employed to calculate transition energies, oscillator strengths, and dipole moments of the ground and excited states of 8VA. The direction of $\Delta\vec{\mu}_{01}$ was assigned in the molecular frame for the lowest optically accessible state. Our study shows that the angle between ground and excited state dipole moment plays a critical role in understanding the change in electronic structure upon optical excitation. Compared to 2AP, 8VA has a larger difference dipole moment which, with twice the extinction coefficient, suggests that 8VA is superior as a two-photon probe for microscopy studies. To this end, we have measured the ratio of the two-photon fluorescence yields of the two analogs by excitation at the respective monomer absorption maxima. We show that 8VA is indeed a significantly brighter two-photon fluorophore, based on our experimental and computational results.

Introduction

Fluorescent base analogs (FBA) of the native bases adenine, cytosine, guanine, and thymine have been used to explore the structure and dynamics of single- and double-stranded nucleic acids including RNA[1] and their interaction with DNA-binding proteins. These include proteins polymerases,[2−4] helicases,[5] and DNA alkyltransferases.[6−9] A large number of studies involving DNA repair proteins include the endonucleases[10−12] and DNA repair proteins.[10,13−17]

8-Vinyladenosine (8VA) (shown in Scheme 1) is an adenosine analogue recently synthesized and characterized by Mély and co-workers.[18−20] It has a high fluorescence quantum yield (0.66 in HEPES buffer)[18] and can be selectively excited when incorporated into DNA because its red-shifted absorption (λ_{max} = 290 nm in water) is well-separated from the absorbance of all other natural nucleic acid bases. Because of it structural similarity to adenine, it can be inserted into DNA without significantly perturbing its double helical base-stacked structure. Recent work by Kenfack et al. showed that 8VA is better stabilized by base stacking than 2-aminopurine (2AP) in dsDNA, and thus they suggest that 8VA is a better probe than 2AP.[19] These characteristics have been exploited to study changes in RNA structure and binding in ricin toxin protein.[21]

SCHEME 1: Synthesis of 8VA

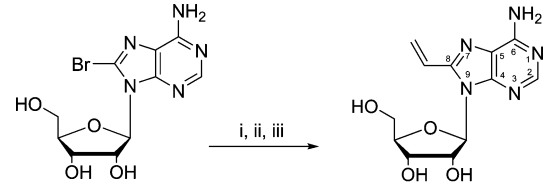

i) HMDS; ii) $(CH_2{=}CH)_4Sn$, $Pd(PPh_3)_4$, NMP; iii) K_2CO_3, CH_3OH

When 8VA is base-stacked in DNA its fluorescence is quenched significantly.[18] This kind of behavior is observed in other fluorescent adenine analogues like 2AP[22−25] and the pteridines 6MAP and DMAP.[26] Several mechanisms have been proposed for explaining fluorescence quenching of 2AP[18,22,27−32] and 8VA[20] in the nucleobase stack, including excited state charge transfer, the presence of dark states, or ground state mixing of orbitals. In 8VA the presence of a vinyl group at C8 acts to increase the degree of conjugation, which in turn should decrease the energy gap between ground and excited states. Recent TD-DFT calculations by Kenfack et al. suggest that there is a significant intramolecular charge transfer in 8VA upon optical excitation.[20] They suggest that fluorescence quenching of 8VA in a dimer or trimer occurs by two possible mechanisms: (1) excited state decay into a low-lying dark state by a nonradiative pathway or (2) orbital

* To whom correspondence should be addressed. E-mail: rstanley@temple.edu.

10.1021/jp908055h
Published on Web 11/25/2009

mixing in the ground state. Possibly both could be involved in fluorescence quenching by base stacking.[20]

Surprisingly, after almost 4 decades of research on FBAs,[33,34] the underlying photophysical processes leading to fluorescence quenching are still unclear. An understanding of the excited state electronic structure of 8VA is necessary to better elucidate the photophysical process involved in its fluorescence quenching. In this work, we have measured the excited state electronic properties such as the difference dipole moment and difference polarizability of 8VA for the lowest energy optical transition using Stark spectroscopy. Stark spectroscopy has been used to explore the excited state electronic structure of several significant photobiological systems, including the photosynthetic reaction center,[35−37] retinal,[38] and DNA photolyase.[39] Additionally, many simpler molecules have been studied whose excited state properties make them useful optical probes, such as coumarin,[40] push−pull systems,[41,42] and many others.[43] We have recently combined state of the art quantum mechanical calculations with absorption Stark spectroscopy to gain insight into the nature of the emissive state of 2AP.[44] In this paper, we have subjected 8VA to a similar analysis and compare its excited state charge distribution to 2AP. Solvatochromism studies were also performed to obtain the solvent response of 8VA.

To complement these results, high level ab initio studies using multiconfiguration self-consistent field (MCSCF), multireference configuration interaction (MRCI), multiconfiguration quasidegenerate second-order perturbation theory (MCQDPT2), and configuration interaction singles (CIS) were done to calculate transition energies, transition dipole moments, as well as ground and excited state dipole moments and the angle between them. The results indicate that the ground and excited state dipoles are antiparallel, suggesting that significant charge transfer occurs upon optical excitation and helps to explain the observed solvatochromism. We also present here finite-field calculations using TD-DFT and CIS methods to calculate the magnitude and direction of the difference dipole moment. The difference dipole moment calculated by computational calculations is in good agreement with the value determined by Stark spectroscopy and consistent with the solvatochromism analysis. The density difference between ground and the bright excited states from these calculations also show significant intramolecular charge transfer character.

Finally, we have determined the ratio of the two-photon absorption (TPA) cross sections, δ, for 8VA and 2AP and can rationalize the result based on the experimental and computational parameters obtained in our study. The results suggest that 8VA shows great promise as a two-photon probe of DNA and should be significantly superior to 2AP in this regard.

Experimental Methods

Synthesis of 8VA. 8-Vinyladenosine was prepared from 8-bromoadenosine using a palladium cross-coupling reaction with tetravinyltin as described by Van Aerschot et al.[45] (Scheme 1). The procedure involves refluxing of 8-bromoadenosine with hexamethyldisilazane (HMDS) in dioxane for 8 h, which yielded persilylated 8-bromoadenosine. The residue was dissolved in *N*-methylpyrolidinone (NMP) and $Pd(Ph_3P)_4$, tetravinyltin was added, and the mixture was heated for 14 h at 110 °C. Purification of the reaction products was facilitated because the presence of the trimethylsilyl ethers allows their extraction in ethyl acetate. The organic solvent (NMP) was removed by washing with water, after which the trimethylsilyl ethers were removed with potassium carbonate in methanol. The final product was purified using a Rainin Dynamax HPLC equipped with a Dynamax (UV-1) UV/vis detector and HP 1050 fluorescence detector. A reverse-phase C-18 column (YMC ODS-AQ, 250 mm × 10 mm) was used in conjunction with a 10−15% gradient of acetonitrile in water with 0.1% formic acid as the mobile phase at a flow rate of 2 mL/min over 20 minutes. The product after purification was characterized by ^{1}H NMR, ^{13}C NMR (data not shown), and by UV/vis spectroscopy using an HP 8452A spectrometer.

Stark Spectroscopy: Experiment and Analysis. The basic setup of the Stark spectrometer is the same as described previously with few modifications.[46,47] The sample cell was constructed from two indium tin oxide (ITO) coated quartz slides having a resistivity of 100 Ω/cm^2. These were oriented with the coatings facing each other and separated by two 55 μM kapton spacers to form an optical capacitor. Twenty-five microliters of the 8VA sample in ethanol was loaded into the optical capacitor before clipping the sample cell onto the coldfinger of the Dewar. The angle of the sample with respect to the polarization of light was varied by rotation of the coldfinger with respect to the probe light.

The Stark spectrometer[44] consists of a 150 W Xe arc lamp whose output was focused using a fused silica lens onto the slit of a $^1/_8$-m monochromator with a 2 nm band-pass. The monochromator was advanced in equal energy steps of 88 cm^{-1}. Any monochromator-induced polarization was scrambled using a depolarizer and subsequently repolarized using a Glan-Taylor polarizer. The probe beam was focused through the fused silica windows of a cryogenic dual reservoir nitrogen optical Dewar (JANIS Research Co) onto the sample cell. The transmitted light was captured and focused with a quartz lens onto a silicon carbide photodiode (sglux GmbH), which is sensitive to light between 220 and 380 nm. The resulting photocurrent was amplified with a Keithley current preamplifier (model 127).

The 217 Hz sinusoidal applied electric field was generated from a Joe Rolfe HV amplifier fed by the sinusoidal output of the lock-in amplifier (SR 830, Stanford Research Systems). Typical field strengths were on the order of 4×10^5 V/cm. Phase-sensitive detection of the field-induced change in transmittance (ΔT) was obtained at 2ω using a 1 s time constant. Usually nine scans were taken and averaged together for a given Stark spectrum.

The low-temperature absorption spectrum was measured using the same setup by substituting an optical chopper for the AC power supply and detecting at ω. The transmittance of both the ethanol reference (I_0) and 8VA in ethanol sample (I) were collected under the same conditions and absorbance spectra were calculated using Beer's law, $A = \log(I_0/I)$.

The analysis of Stark spectra derives from Liptay's approach.[43] The field-modulated spectrum can be fitted to derivatives of the zero-field absorption spectrum. The energy-weighted field-induced change in the extinction can be given as

$$\frac{\Delta\varepsilon}{\tilde{\nu}} = (f_c\vec{F})^2\left\{A_\chi\frac{\varepsilon(\tilde{\nu})}{\tilde{\nu}} + \frac{B_\chi}{15ch}\frac{\mathrm{d}(\varepsilon(\tilde{\nu})/\tilde{\nu})}{\mathrm{d}\tilde{\nu}} + \frac{C_\chi}{30c^2h^2}\frac{\mathrm{d}^2(\varepsilon(\tilde{\nu})/\tilde{\nu})}{\mathrm{d}\tilde{\nu}^2}\right\} \quad (1)$$

The term $\varepsilon(\tilde{\nu})$ represents the energy-weighted unperturbed extinction coefficient as a function of the energy $\tilde{\nu}$, $\vec{F}$ represents the electric field applied on the sample, and f_c is the local field correction factor for the solvent cavity. The constants c and h are the speed of light and Planck's constant, respectively. An enhancement of the applied field is expected due to the cavity

field of solvent matrix. Because of this, f_c is always greater than 1.[48] The local field correction factor was estimated to be $f_c = 1.21$ using the ratio of experimentally determined $\Delta\vec{\mu}$ from Stark spectroscopic analysis and $\Delta\vec{\mu}$ calculated from vacuum computational studies. χ defines the angle between the direction of electric field vector of the linearly polarized light and that of the applied electric field F. All the Stark experiments reported here were performed with $\chi = 54.7°$ (magic angle) or $\chi = 90°$, after correcting for the refractive indices of liquid nitrogen and the ITO-coated quartz slides.

The derivative scaling factors A_χ, B_χ, C_χ are related to intrinsic electronic properties of the chromophore. The A_χ term represents the transition moment polarizability and hyperpolarizability, reflecting the influence of the electric field on the transition moment. In part, A_χ reflects the field-induced orientation or poling of a molecule possessing a ground state dipole moment. A rigid environment immobilizes the molecules; therefore, $A_\chi \sim 0$. Information about the change in polarizability and the change in permanent dipole moment can be obtained from the coefficients B_χ and C_χ. The B_χ term is related to change in the transition state polarizability, where

$$B_\chi \sim \frac{5}{2}\mathrm{tr}(\Delta\vec{\alpha}) + (3\cos^2\chi - 1)\left(\frac{3}{2}\vec{m}\Delta\vec{\alpha}\vec{m} - \frac{1}{2}\mathrm{tr}(\Delta\vec{\alpha})\right) \quad (2)$$

Here $\vec{m}$ is the transition dipole moment. The difference polarizability, $\Delta\vec{\alpha} = \vec{\alpha}_e - \vec{\alpha}_g$, is a tensor, but for our purpose we consider only the trace of this polarizability, $\mathrm{tr}(\Delta\vec{\alpha})$, which is a scalar representing the polarizability volume. The trace of a tensor is invariant with respect to a change in coordinate system. Thus, $\mathrm{tr}(\Delta\vec{\alpha})$ is a good estimate of the change in the polarizability volume upon excitation.

The applied electric field will produce a second-derivative component of the absorption spectrum when the difference dipole moment, $\Delta\vec{\mu}$, is nonzero:

$$C_\chi = |\Delta\vec{\mu}|^2\{5 + (3\cos^2\chi - 1)(3\cos^2\zeta_A - 1)\} \quad (3)$$

where ζ_A represents the angle between $\Delta\vec{\mu}$ and transition dipole moment $\vec{m}$, $\zeta_A^{0n} = \angle\vec{\mu}_{0n}, \vec{m}_{0n}$ for the $S_0 \rightarrow S_n$ transition. When χ is the magic angle (54.7°) all the χ-dependent values vanish and $\mathrm{tr}(\Delta\vec{\alpha})$ and $\Delta\vec{\mu}$ can be obtained directly.

Fitting the Stark spectra begins with an analysis of the low-temperature absorption spectrum. The low-temperature absorption spectrum was fitted to a linear combination of Gaussian functions. Analytical derivatives of these Gaussians provide much smoother numerical derivatives than taking numerical derivatives of the experimental spectrum. These derivatives are fitted to the corresponding part of the Stark spectrum by varying the A_χ, B_χ, and C_χ coefficients. For an optimum fit, both the absorption and Stark spectral parameters were allowed to vary and the spectra were fitted simultaneously. The fit was weighted equally between both the spectra. To find a robust set of coefficients, Stark spectra at several fields and at least two different angles of χ were used. Six data sets were obtained for each angle of χ, and each set of data was individually fitted. All the determined values of $\Delta\vec{\mu}$ and $\mathrm{tr}(\Delta\vec{\alpha})$ are reported in terms of debye and Å^3, respectively, where 1 D = 3.36×10^{-30} C m and 1 Å^3 = 1.113×10^{-40} C m^2/V.

Solvatochromism: Experiment and Analysis. Methanol, ethanol, butanol, dimethyl sulfoxide (DMSO), dimethylformamide (DMF), dioxane, tetrahydrofuran (THF), ethyl acetate, toluene, benzene, chloroform, and dichloromethane were spectroscopic grade and used as received. HPLC grade water and acetonitrile were used as received. A 0.40 cm × 1.0 cm fluorescence quartz cell was used. The maximum optical density of the 8VA solution was approximately 0.01.

Excitation and emission spectra of 2 μM solutions of 8VA in each of these solvents were taken using a SPEX FluoroMax-2 fluorimeter. The excitation spectra were collected with the emission wavelength set to 380 nm and the emission spectra were collected with excitation at 300 nm unless otherwise noted. All spectra were collected with a total integration time of 0.4 s, 1 nm step size, and 2 nm band-pass for both the excitation and emission monochromators. The spectra were solvent corrected by subtracting excitation and emission spectra of the corresponding solvent. All spectra were corrected for any wavelength bias of the fluorimeter.

The Ooshika−Lippert−Mataga (OLM) equation defines the correlation between the solvent-dependent absorption and emission frequencies at their maximum intensities and the solvent properties as shown in eqs 4 and 5:[49]

$$\tilde{\nu}_{abs} - \tilde{\nu}_{em} = \frac{2F(\varepsilon,n)}{hca^3}(\vec{\mu}_e - \vec{\mu}_g)^2 + C = \frac{2F(\varepsilon,n)}{hca^3}|\Delta\vec{\mu}|^2 + C \quad (4)$$

where $\tilde{\nu}_{abs}$ and $\tilde{\nu}_{em}$ are the frequencies of the peak absorbance and fluorescence respectively, h is Planck's constant, c is the velocity of light in vacuum, and a is the radius of the solvated fluorophore including the first solvation sphere. The dielectric properties of the solvent are found in the $F(\varepsilon,n)$ term:

$$F(\varepsilon,n) = f(\varepsilon_0) - f(n) = \frac{\varepsilon_0 - 1}{2\varepsilon_0 + 1} - \frac{n^2 - 1}{2n^2 + 1} \quad (5)$$

where n is the solvent refractive index and ε_0 is the dielectric constant. This treatment ignores the polarizability of the fluorophore and assumes that the ground and excited states dipole moments point in the same direction.

If one assumes the polarizability of the fluorophore is the same as the solvent and that $\vec{\mu}_g$ and $\vec{\mu}_e$ point in different directions, then eq 4 will become[49−52]

$$\tilde{\nu}_{abs} - \tilde{\nu}_{em} = \Delta b f(\varepsilon,n) + C \quad (6)$$

where

$$f(\varepsilon,n) = \left[\frac{\varepsilon - 1}{\varepsilon + 2} - \frac{n^2 - 1}{n^2 + 2}\right]\frac{2n^2 + 1}{n^2 + 2} \quad (7)$$

and

$$\Delta b = \frac{2}{hca^3}(|\vec{\mu}_g{}^2| + |\vec{\mu}_e{}^2| - 2|\vec{\mu}_g||\vec{\mu}_e|\cos\theta) \quad (8)$$

This more general treatment is due to Bilot and Kawski[53] based on Bakhshiev's analysis.[51] Here, θ is the angle between $\vec{\mu}_g$ and $\vec{\mu}_e$. A plot of the Stokes shift $(\tilde{\nu}_e - \tilde{\nu}_g)$ vs the solvent

polarization function $f(\varepsilon,n)$ is obtained and the slope of the eq 7 is used to determine the excited state dipole moment, $\vec{\mu}_e$, from eq 8, based on an estimate of $\vec{\mu}_g$ from computational methods.

Two-Photon Fluorescence Measurements. Stirred micromolar solutions of 2Ap riboside (500 μM) and 8VA (350 μM) in 50 mM potassium phosphate buffer, pH 7.0 at 25 °C were subjected to ca. 200 fs pulses of light with and energy of about 200 nJ/pulse at a repetition rate of 1 kHz. The pulse train was generated by a Ti:sapphire-pumped nonlinear optical parametric amplifier (NOPA) of home design centered at about 1200 nm.[54] Excitation at 603 nm was generated by second-harmonic generation in a 4 mm thick type-I BBO crystal. The residual infrared light was removed by an infrared absorption filter. The fused silica fluorescence cuvette had 1 cm × 0.4 cm inner dimensions and four clear optical windows. The NOPA output was focused with an 8 cm focal length lens along the 1 cm path length of the cuvette. The fluorescence was collected at 90° with a 2.54 cm diameter 4 cm focal length quartz lens through the 0.4 cm dimension of the cuvette to minimize any inner filter effect. The collimated fluorescence was focused onto the 400 μm slit of a Digikrom 0.24 m spectrograph filtered through a blue band-pass filter whose transmission was relatively flat over the range of both 2AP and 8VA emission. The emission was detected with an integration time of 15 s using an Andor CCD camera cooled to −70 °C.

The two-photon absorption (TPA) cross section for noncentrosymmetric molecules can be given as[55]

$$\delta = \frac{32\pi^4 g_{max}}{15c^2h^2}|\vec{m}_{01}|^2|\Delta\vec{\mu}_{01}|^2(2\cos^2\zeta_A + 1) \qquad (9)$$

where g_{max} is the maximum in the line width function, $\vec{m}_{01}$ is the transition dipole moment, $\Delta\vec{\mu}_{01}$ is the difference dipole moment, and ζ_A is the angle between $\vec{m}_{01}$and $\Delta\vec{\mu}_{01}$. δ is expressed in Goeppert−Mayer (GM) units (1 GM = 10^{-50} cm^4 s photon^{-1} molecule^{-1}). It can be seen that δ is directly proportional to the product of the squares of the $\vec{m}_{01}$ and $\Delta\vec{\mu}_{01}$. $|\vec{m}_{01}|^2$ is proportional to the oscillator strength, which is in turn proportional to the integrated extinction, $\int\varepsilon_i\,d\nu$. This can be estimated from the integrated absorption spectrum of the $S_0 \rightarrow S_1$ transition. Since $\Delta\vec{\mu}_{01}$ is the measure of charge displacement, the magnitude of δ depends on the degree of intramolecular charge transfer (ICT) upon excitation.

The two-photon *action* cross section is defined as $\eta_i\delta_i$, where η_i is the fluorescence quantum yield of molecule i. Absolute action cross sections are difficult to measure, but the ratio of the δ of two different fluorophores i and j can be obtained simply by taking the ratio of their measured two-photon-induced fluorescence at the same (or close to the same) excitation wavelengths. If the η are known independently, then δ_i/δ_j for the ith and jth fluorophores is

$$\frac{\delta_i}{\delta_j} = \frac{\eta_j c_j}{\eta_i c_i}\frac{\int I_i\,d\nu}{\int I_j\,d\nu} = \frac{|\vec{m}^i_{01}|^2|\Delta\vec{\mu}^i_{01}|^2(2\cos^2\zeta^i_A + 1)}{|\vec{m}^j_{01}|^2|\Delta\vec{\mu}^j_{01}|^2(2\cos^2\zeta^j_A + 1)} \qquad (10)$$

where I_i and I_j are the two-photon-induced fluorescence intensities at concentrations c_i and c_j, respectively.

Theoretical Methods. In this section, we present the theoretical methods used in this report, beginning with approaches utilizing a complete active set (CAS) of molecular orbitals to generate wave function expansions. Time-dependent density functional theory (TD-DFT) calculations of the excited states of 8VA using a polarizable continuum model (PCM) for solvent interactions, including the influence of finite external electric fields, were also performed. State-averaged multiconfiguration self-consistent field (SA-MCSCF) and MCQDPT2 calculations were carried out using GAMESS, version 24 MAR 2007 (R3),[56] and the COLUMBUS Quantum Chemistry Program Suite.[57−59] Multireference configuration-interaction (MRCI) calculations were carried out using COLUMBUS. Møller−Plessett second-order perturbation theory MP2, TD-DFT, and finite-field calculations were performed using the Gaussian 07W program (ver. c02).[60]

MCSCF, MRCI, and MCQDPT2 Calculations. The geometry for 8VA is the ground state minimum optimized with MP2 and the cc-pVDZ atomic orbital basis set,[61] constrained to C_S symmetry. In the true ground state (GS) geometry, amino pyramidalization would break C_S symmetry; however, this geometric difference has little effect on the excited state energies or character in 8VA, as has been seen before in other amino-substituted bases,[62] and within the CAS-based calculations presented here C_S symmetry affords a larger wave function expansion. The conformer chosen has the vinyl group syn to the amino group, since this orientation is likely to be the most stable in the nucleoside.[18]

Molecular orbitals (MOs) were obtained from a SA-MCSCF procedure averaged over a maximum of eight singlet states. The CAS for most calculations presented here (12 maximum orbitals) contained only π MOs since the two lowest $\pi\rightarrow\pi^*$ transitions were the primary focus. Core, σ, and the nitrogen lone pair (n_N) MOs were kept as doubly occupied. One calculation included two n_N MOs in order to locate $n_N\pi^*$ states in relation to the $\pi\pi^*$ states.

The CAS was occupied with up to 14 electrons in 12 MOs, denoted as (14,12), where (n,m) denotes n electrons in m active orbitals. Up to about 70 000 reference configuration state functions (CSFs) were generated from the SA-MCSCF calculations. Further refinement was achieved for a (12,11) MCSCF calculation at the Multiconfiguration Quasidegenerate Second-Order Perturbation Theory (MCQDPT2) level.

MRCI calculations were also performed where all core and σ MOs were maintained as frozen and single-excitations were allowed from a (14,11) CAS to the virtual orbitals, generating up to about 10 million CSFs in the MRCI expansion. Details and justification for the specific choice of CAS in each case are explained in the Computational Results section. Energies, static state dipoles, and transition dipoles were calculated at both the SA-MCSCF and MRCI level. Only singlet states were calculated, with S_i defined as the ith excited singlet state relative to the GS, S_0.

Finite-Field Calculations. Difference dipole moments, $\Delta\vec{\mu}_{0n}$, were calculated using the finite-field hexapole method, where an external electric field propagating along the $\pm x$, $\pm y$, and $\pm z$ directions in the center of mass coordinates is applied in silico. $\Delta\vec{\mu}_{0n}$ is defined as the vector difference between the static state dipole of state n and the GS dipole, $\Delta\vec{\mu}_{0n} = \vec{\mu}_n - \vec{\mu}_0$. The finite-field calculations were done at two different field intensities, 0.001 and 0.0005 au, to verify that the influence of the electric field on the transition energy was linear and no higher order effects were present.

For the TD-DFT based calculations, the geometries were optimized at the B3LYP/6-311+G (d,p) level of theory. The minimum energy structure was further confirmed by calculating vibrational frequencies at the same level of theory. The excited

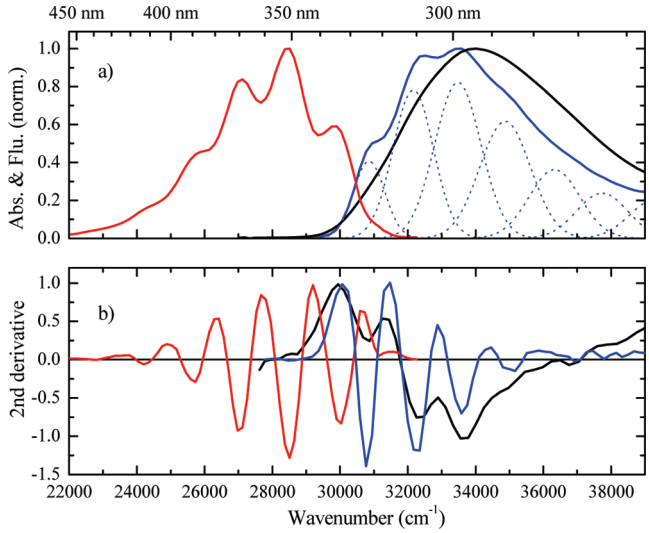

Figure 1. (a) Normalized room temperature (black line) and 77 K absorption (blue line) spectra, of 1 mM 8VA in ethanol, including the low-temperature deconvolution using seven Gaussians (dashed blue line). The 77 K fluorescence spectrum (red line) is also shown. (b) Normalized numerical second derivatives of the spectra in part a. The energy difference between minima for all three conditions is 1460 cm^{-1}.

state energies, transition moments, and excited state dipole moments were calculated at the B3LYP/6-311+G(d,p) level of theory. For CIS calculations the geometry was optimized at the MP2/6-311+G(d,p) level of theory. The polarizable continuum model, developed by Tomasi et al.,[63,64] was used to include the effect of the dielectric response of the solvent (e.g., water, ethanol) on $\Delta\vec{\mu}_{0n}$. The difference electron density was calculated by subtracting the SCF ground state density from the one-particle ρ-density for the corresponding excited states. Chemcraft (http://www.chemcraftprog.com) was used to generate and visualize the excited state dipole moment vectors and difference density.

The calculated Stark shift under the applied static electric field F is given by $E(F) = E(0) - \sum_i \Delta\mu_i F_i - 1/2\sum_{i,j}\Delta\alpha_{i,j}F_iF_j$, where E is the vertical excitation energy and $\Delta\mu_i$ and $\Delta\alpha_{i,j}$ are the vector and tensor components, respectively, of the change in the dipole moment upon optical excitation and the excess polarizability in the i and i, j directions. The excess polarizability is often discussed via its isotropic tr($\Delta\alpha_{i,j}$) value.

Results

Low-Temperature and Room-Temperature Absorption and Emission Spectra. The low-temperature (77 K) absorption and emission spectra and room-temperature (298 K) absorption spectrum of 1 mM 8VA in ethanol are showed in Figure 1a. All spectra have been peak normalized. Vibronic analyses (as discussed below) for the 298 and 77 K absorption and 77 K emission spectra are presented in Table 1.

At room temperature, the $S_0 \rightarrow S_1$ transition spans from 30 000 to about 39 000 cm^{-1} with a maximum at 34 014 cm^{-1} (294.0 nm) (Figure 1a, black line). A second electronic transition is observed growing in above 39 000 cm^{-1} but is not the subject of this study. The numerical second derivative of the 298 K absorption spectrum is shown in Figure 1b (black line). The evenly spaced well-structured derivative spectrum suggests a vibronic progression. The energy difference between successive minima is about 1460 ± 93 cm^{-1}.

At low temperature, the vibronic features in the absorption spectrum are better resolved (Figure 1a, blue line). The low-temperature absorption spectrum has a maximum at 33 579 cm^{-1} (297.8 nm), with a red shift of 435 cm^{-1} relative to the 298 K maximum, similar to that observed for the adenine analog 2AP.[46] The evident vibronic structure afforded a spectral deconvolution using seven Gaussian functions (blue dashed line). This deconvolution was supported by an analysis of the numerical second derivative of the 77 K absorption spectrum (Figure 1b, red line), which reveals a single vibronic progression with an energy spacing of 1465 ± 101 cm^{-1}. This energy spacing is identical, within experiemental error, to both the room- and low-temperature peak analyses.

The emission spectrum of 8VA at 77 K in ethanol (Figure 1a, blue line) clearly shows mirror image symmetry with the corresponding absorption spectrum. The second derivative of the emission spectra is shown in Figure 1b (blue line). From the second-derivative analysis the emission maximum is observed at 28 506 cm^{-1} (350.8 nm), a Stokes shift of −5073 cm^{-1}. Again, a clear vibronic progression is seen, with an energy spacing of 1459 ± 140 cm^{-1}. This value is identical with that obtained from the absorption spectra, suggesting that vibrational spacings in the S_0 and S_1 states, and hence the nuclear geometries, are nearly the same, at least for this nuclear coordinate.

Stark Spectroscopy Results. The energy-weighted 77 K Stark spectra of 1 mM 8VA in frozen ethanol glass at two different values of χ are shown in Figure 2a. The Stark spectra show a dependence on χ, indicating that $\zeta_A \neq 54.7°$ but must be somewhat smaller.

TABLE 1: Vibronic Analysis of 8VA Absorption and Emission Spectra (band positions in cm^{-1})

band	Abs_{298K}	Abs_{77K}	Em_{77K}
1	27 624	28 481	22 805
2	30 864	30 767	24 195
3	32 258	32 349	25 727
4	33 557	33 579	26 976
5	36 765	35 162	28 506
6	NA	36 920	30 030
7	NA	37 799	31 143
$\Delta\bar{\nu}_{av}$[a]	1460 ± 93	1465 ± 101	1456 ± 140

[a] Energy difference between adjacent bands.

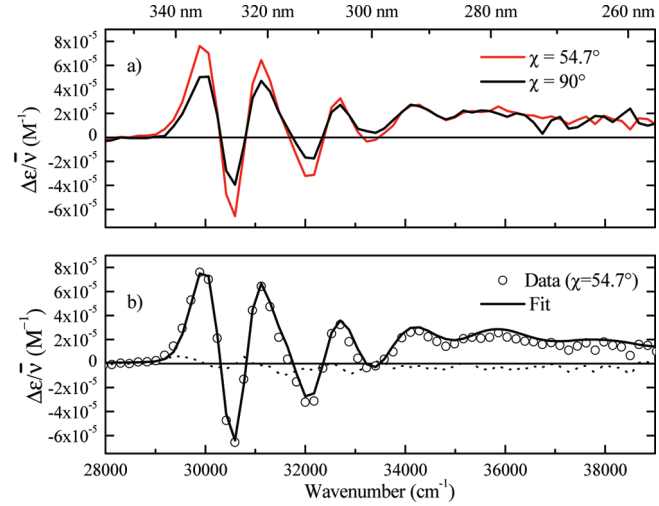

Figure 2. (a) Energy-weighted Stark spectra of 8VA in ethanol at 77 K taken at $\chi = 54.7°$ (red line) and 90° (black line). (b) A comparison of the $\chi = 54.7°$ data (○) and the fit (black line). The residuals from the fit are shown as a dashed line.

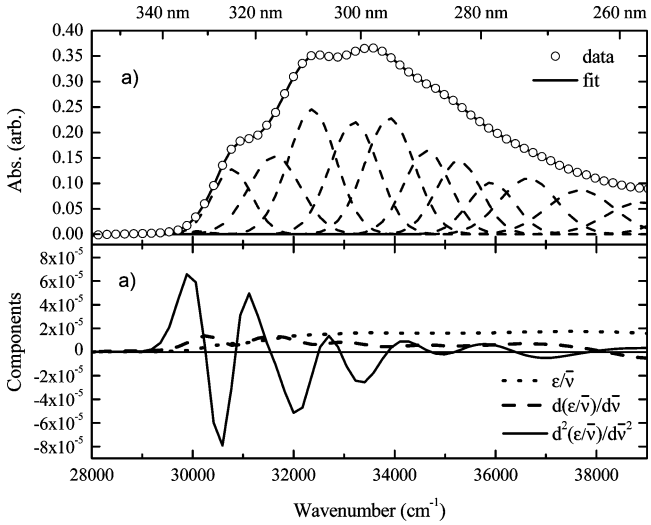

Figure 3. (a) Final set of Gaussian functions (− −) from the simultaneous fit of the 77 K 8VA absorption (data ○) and Stark spectra. (b) Summed zeroth (- -), first (− −), and second (—) derivative components of the absorption spectrum used to fit the Stark spectrum ($\chi = 54.7°$).

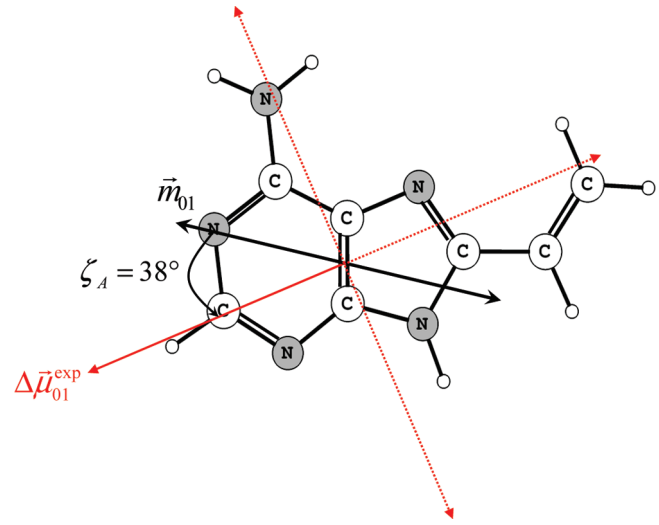

Figure 4. Possible orientations of $\Delta\vec{\mu}_{01}$(red vectors) from the Stark analysis. The orientation that is consistent with the calculations is shown as a solid vector. The transition dipole moment is shown for reference (black vector).

TABLE 2: Stark Results (field corrected, $f_c = 1.21$)

$\Delta\vec{\mu}_{01}^{exp}$ (D)	tr($\Delta\vec{\alpha}_{01}$) (Å^3)	ζ_A
4.7 ± 0.3	21 ± 11	38° ± 6°

Figure 2b shows the $\chi = 54.7°$ Stark spectrum (○) and a fit using the derivatives of the absorption spectrum (black line). The residuals to the fit are also shown (dashed line). This fit was accomplished by calculating the zeroeth, first, and second derivatives of Gaussian-deconvolved low-temperature absorption spectrum, and weighting these components by the A_χ, B_χ, and C_χ coefficients, respectively. A simultaneous fit of the absorption spectrum was performed by making small adjustments to the seven Gaussians. A simultaneous fit using 14 Gaussians was also performed. This is equivalent to assigning two Gaussians to each vibronic band and resulted in a better overall fit. However, both approaches gave the same electronic structure parameters, within about 10%.

The final result of this process is shown in Figure 3, which shows the 14 Gaussian functions used to fit the absorption spectrum (a), and the sum of their zeroth, first, and second derivatives to fit the Stark spectrum (b). A comparison of the spectra (Figure 2) with the second derivative of the absorption spectra (Figure 3b) shows that the difference dipole component dominates the overall Stark spectrum. An evaluation of the C_χ term (eq 3) gives a $\Delta\vec{\mu}_{01}$= 4.7 ± 0.3 D for the lowest optically accessible transition after applying the local field correction. The change in the polarizability, tr($\Delta\vec{\alpha}_{01}$) = 21 ± 11 Å^3. The angle between the difference dipole moment and the transition dipole moment is $\zeta_A^{01} = 38 \pm 6°$. These results are summarized in Table 2.

The orientation of $\Delta\vec{\mu}_{01}$ is defined relative to $\vec{m}_{01}$ through ζ_A. This means that there are an infinite number of possible orientations for $\Delta\vec{\mu}_{01}$ which lie on a cone at ζ_A about $\vec{m}_{01}$. If we make the plausible assumption that charge displacement for the $\pi \rightarrow \pi^*$ transition occurs in the plane of 8VA, then the number of possible orientations becomes four. Three of these four possible vectors are shown in Figure 4 as red dashed lines drawn from the center of mass of 8VA. For reference, the $S_0 \rightarrow S_1$ transition dipole moment vector, $\vec{m}_{01}$, is shown as a black double-headed arrow (not drawn to scale). We have indicated the particular $\Delta\vec{\mu}_{01}$ that agrees best with the ab initio calculations as a solid red vector.

The Stark analysis was done assuming that there was no contribution from the $S_0 \rightarrow S_2$ transition below 40 000 cm^{-1}. The assumption that there is no overlap between the $S_0 \rightarrow S_1$ and $S_0 \rightarrow S_2$ transitions is reasonable on the basis of the computational analysis (see below). However, an analysis of the Stark spectra with the assumption of an overlapping transition up to 39 000 cm^{-1} did not change our results significantly (analysis not shown). Both the sum of the derivatives of the absorption spectrum and Stark spectra become structureless above ~40 000 cm^{-1}, probably due to spectral congestion.

Solvatochromism Results. The excitation spectra of 2 μM 8VA in various solvents are shown in the Supporting Information, Figure S1, and the results are tabulated in Table 3. Generally, a blue shift was observed as a function of increasing solvent polarity. The excitation line shape was essentially unchanged as a function of polarity (the line shapes in benzene and toluene were truncated at the blue edge due to absorption by the solvent in this range). The solvatochromic shift seems to be relatively independent of whether the solvent can form hydrogen bonds, although water has the largest shift, λ_{max} = 297 nm. This kind of blue shift was also observed in the case of 2AP in water, suggesting that H-bonding with water stabilizes the ground state more than the excited state.[25,27] Interestingly, chloroform shows nearly as large a blue shift as water (299 nm). DMF and DMSO both show a smaller blue shift than might be expected for the polarity of these solvents. Both molecules can act as H-bond donors but not acceptors.

The emission spectra of 8VA in various solvents are shown in Supporting Information, Figure S2. The emission spectrum in water was significantly more red-shifted (λ_{max} = 388 nm) compared to all other solvents used. In the least polar solvents, the emission maxima shifted toward the blue (e.g., toluene λ_{max} = 372 nm and for benzene λ_{max} = 374 nm). In general, emission red-shifted with increasing solvent polarity (see Table 3). To check for an excitation wavelength dependence, the emission spectra of 8VA in water was collected at 280, 290, 300, 310, and 320 nm excitation wavelengths, respectively (data not shown). The line shapes of these emission spectra showed no dependence on excitation wavelength.

TABLE 3: Solvent-Dependent Stokes Shift of 8VA

solvent	$f(\varepsilon,n)$	λ^{ex}_{max} (nm)	$\tilde{\nu}^{ex}_{max}$ (cm^{-1})	λ^{em}_{max} (nm)	$\tilde{\nu}^{em}_{max}$ (cm^{-1})	$\Delta\tilde{\nu}$ (cm^{-1})
benzene	0.0057	308	32 467	374	26 738	5729
toluene	0.029	307	32 573	372	26 882	5692
dioxane	0.042	309	32 363	378	26 455	5907
diethylether	0.365	306	32 680	376	26 596	6084
chloroform	0.377	299	33 444	375	26 667	6778
THF	0.550	309	32 363	380	26 316	6047
dichoromethane	0.590	301	33 223	374	26 738	6485
n-butanol	0.753	306	32 680	381	26 247	6433
ethanol	0.813	304	32 895	381	26 247	6648
DMF	0.836	312	32 051	381	26 247	5805
DMSO	0.840	312	32 051	381	26 247	5805
methanol	0.854	302	33 113	380	26 316	6797
acetonitrile	0.859	302	33 112	378	26 455	6657
water	0.913	297	33 670	388	25 773	7897

An increase in the Stokes shift was observed as the polarity of the solvent increased. The maximum Stokes shift was observed for water (~7900 cm^{-1}) and the minimum shift was observed for benzene or toluene (~5700 cm^{-1}). A large change in the Stokes shift of 8VA as a function of solvent (~3200 cm^{-1}) from benzene to water suggests that there is a significant electronic redistribution occurring in the excited state of the 8VA.

The solvatochromism analysis was performed using the method of Bakhshiev[51] which, unlike the Lippert−Mataga equation, does not assume that the ground and excited state dipoles are parallel. A plot of ($\tilde{\nu}_{abs} - \tilde{\nu}_{em}$) vs $f(\varepsilon,n)$ from eq 6 is showed in Figure 5. To obtain $\vec{\mu}_e$ from this analysis, the slope of $\Delta b = 982$ cm^{-1} from the linear fit was used in eq 8, along with $\vec{\mu}_g = 3.1$ D (and its direction) from ab initio calculations. The (Onsager) radius, $a = 5.7$ Å, was calculated from the PCM model. Therefore, the angle between $\vec{\mu}_0$ and $\vec{\mu}_1$ (average angle 162° ± 11°) was used to determine the magnitude of $\vec{\mu}_1$, which was 1.3 ± 0.2 D. This value is consistent with the computational and Stark spectroscopy analyses.

Computational Results. The calculated absorption spectrum of 8VA in vacuum using TD-DFT/B3LYP/6-311+G(d,p) is shown in Supporting Information, Figure S3. A B3LYP/6-311+G (d,p)-optimized geometry was used as the starting structure for TD-DFT calculations and an MP2/6-311+G(d,p)-optimized geometry was used for CIS calculations with the same basis set. The lowest energy transition occurs at 310 nm. This compares well with the excitation spectral maxima in benzene, 308 nm, the most nonpolar solvent used.

The HOMO, LUMO, and the difference density between excited and ground states from TD-DFT calculations are shown in Figure 6 (note that the same results, not shown, from CIS calculations are not significantly different from the TD-DFT approach). The lowest electronic transition is primarily a

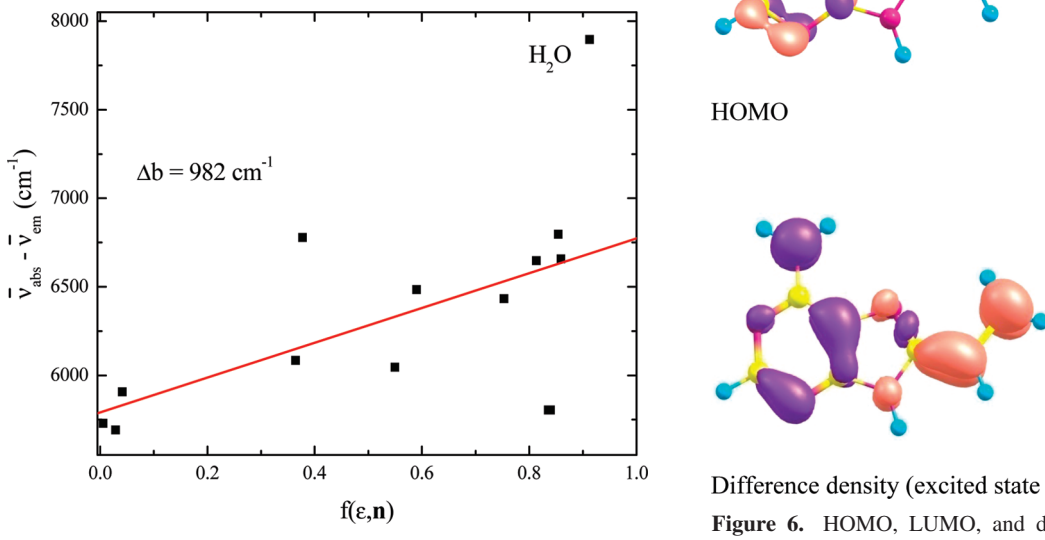

Figure 5. Analysis of solvatochromism of 8VA using the method of Bakhshiev. All points were included in the linear fit. The slope, Δb, equals 982 cm^{-1}. The large Stokes shift for water is indicated.

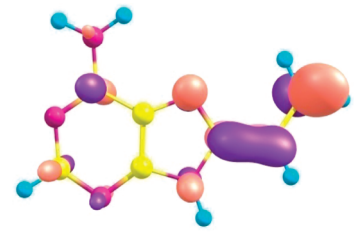

LUMO

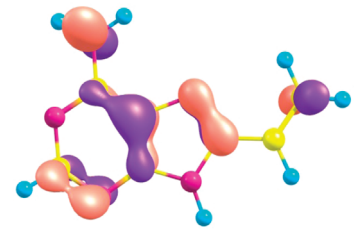

HOMO

Difference density (excited state density - ground state density)

Figure 6. HOMO, LUMO, and difference density for the $S_0 \rightarrow S_1$ transition calculated using TD-DFT/B3LYP/6-311+G(d,p). Purple indicates lower electron density, while red indicates regions of higher electron density.

TABLE 4: $\Delta\vec{\mu}_{01}^{exp}$ Values in Vacuum, Ethanol, Water Calculated Using the Finite Field Method

$\Delta\vec{\mu}_{01}^{c}$ (D)	vacuum	EtOH	water
TD-DFT/B3LYP/6-311+G(d,p)	6.48	7.30	7.37
TD-DFT/BHandHLYP/6-311+G(d,p)	4.84	4.96	4.97
CIS/6-311+G(d,p)	3.79	3.86	3.86

HOMO→LUMO transition (65%). The electron density in the HOMO is mostly centered on the six-membered ring of the purine, but in the LUMO the electron density switches almost completely to the C_8-C_{10} bond and C_{11}, the terminal vinyl carbon. This is seen more clearly by examining the difference density between the excited S_1 and ground S_0 states, which shows that electron density is transferred from the purine ring to the vinyl group upon optical excitation.

A quantitative evaluation of $\Delta\vec{\mu}_{01}$ is obtained from the finite-field calculations, using TD-DFT (B3LYP and BHandHLYP functionals) and CIS methods with a 6-311+G (d,p) basis set. The magnitude of difference dipole moment $\Delta\vec{\mu}_{01}$ for various solvents is given in Table 4. The direction of $\Delta\vec{\mu}_{01}$ is shown in Figure 7 in comparison with the Stark result that matches most closely. It can be seen that the difference dipole moment direction calculated by either method agrees well with the experimental result and points in the direction opposite the vinyl group, as expected from considering the difference electron density for the HOMO→LUMO transition. However, the B3LYP calculation overestimates the degree of charge transfer, a result that has been observed by others.[65] The BHandHLYP functional reproduces the magnitude of the difference dipole moment of 8VA within experimental error and is about 2 D smaller than the B3LYP calculation.

Higher level ab initio calculations were performed to better understand the nature of the optically allowed transition. Energies and transition data are given in Table 5 (only values for S_1 and S_2 are given). We define θ_{mCC} as the angle between the transition dipole corresponding to the brightest excitation and the C_4-C_5 double bond shared by the two rings of 8VA (Table 5). Calculated values for θ_{mCC} varied from about 80° to about 104°. In order to locate the n_N,π^* states in relation to the GS and π,π^* states, an eight-state SA-MCSCF calculation followed by MRCI with four A′ (GS and π,π^*) and four A″ (n_N,π^*) states and a (14,11) CAS was carried out. The CAS contained nine π and two n_N MOs. S_1, S_2, and S_5 are π,π^* states (A′) with energies 5.38, 5.47, and 6.43 eV, respectively, at the MRCI level. At this level, the S_1 state is predominately HOMO→LUMO in character, with S_2 being of more mixed π MO character. MRCI tends to stabilize $\pi\pi^*$ states compared to

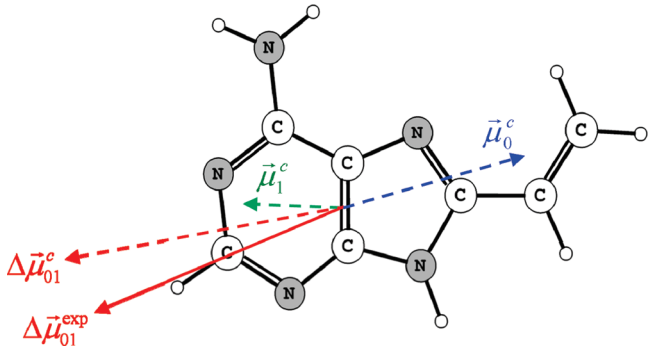

Figure 7. The directions of the calculated ground state dipole moment $\vec{\mu}_0^c$, excited state dipole moment $\vec{\mu}_1^c$, and difference dipole moment $\Delta\vec{\mu}_{01}^c$ in the 8VA molecular frame (dashed vectors). The experimentally determined difference dipole, $\Delta\vec{\mu}_{01}^{exp}$ is shown as a solid red vector.

MCSCF due to increased dynamical correlation, and this can be seen in Table 5, where the MCSCF results are shown as well. The A″ excited state energies at the MRCI level were 6.09, 6.32, 6.89, and 8.01 eV for S_3, S_4, S_6, and S_7, respectively, placing the first n_N,π^* state about 0.5 eV higher in energy than the S_2 π,π^* state.

Since the n_N,π^* states were found to be well-separated energetically from the first two π,π^* states, we focused on obtaining better excitation energies and properties for the π,π^* states. For this purpose, the first three A′ states were calculated using a (12,11) CAS containing all of the π MOs with MCSCF followed by MCQDPT2. It has been shown before that π,π^* states of purine bases are described best with MCSCF when all π MOs are included in the active space followed by perturbation theory.[66] Results are shown in Table 5. The MCQDPT2 excited state energies are 4.35 eV for S_1, which is the bright HOMO,LUMO state, and 4.77 eV for S_2, which is a dark state of mixed π,π^* character. Both the energies and the order of these two π,π^* states are very dependent on the degree of both static and dynamical correlation. Most importantly, the ordering of the bright and dark states switches in going from MCSCF to MCQDPT2, with the bright state being assigned to S_1 at the MCQDPT2 level since this state is primarily HOMO,LUMO in character, which is in agreement with the TD-DFT results. Oscillator strength calculations are not currently available at the MCQDPT2 level in GAMESS. The oscillator strengths between the GS and the first two excited states were calculated at the MCSCF and MRCI levels (Table 5). The oscillator strengths, f_{0n} ($n = 1, 2$), given next to the S_1 and S_2 energies, refer to the transition between the GS and the particular excited state. In general, the transition with higher f_{0n} corresponded to the transition from the GS→π,π^* state containing the most amount of HOMO→LUMO character. However, whether that state was S_1 or S_2 varied, depending on method and CAS. This is likely because the energy of the π,π^* states is affected by the amount of both static and dynamical correlation, with the HOMO,LUMO state affected more than the other π,π^* states. So, in most cases MCSCF predicts that the S_2 is the bright state while adding correlation switches this. Although we cannot calculate oscillator strengths with MCQDPT2, inspection of the wave function shows that perturbation correction switches the ordering of S_1 and S_2. It should be noted, however, that in the case of MCSCF and MRCI using a (14,11) CAS containing only nine π MOs, both S_1 and S_2 have significant HOMO,LUMO character, and the oscillator strengths corresponding to excitations from the GS to these states are very similar in magnitude, presumably because the states are predicted to be very close in energy and can mix.

Static dipole moments were calculated at the MCSCF and MRCI levels since they could not be calculated at the MCQDPT2 level (see Table 6). We define $|\Delta\vec{\mu}_{0n}|$ as vector difference between the GS dipole moment, $\vec{\mu}_0$, and the bright, predominantly HOMO→LUMO, π,π^* state dipole $\vec{\mu}_1$ or $\vec{\mu}_2$ given in Table 5. $|\Delta\vec{\mu}_{0n}|$ is largely independent of the CAS or method, although the brighter state varied between S_1 and S_2, depending on the method as explained above. The angle between ground and excited state dipole moments was found to lie between 162° and 167°, which lends support to one of the four experimentally determined ζ_A values presented in this report (see Figure 7).

Two-Photon Action Cross Section Ratio of 8VA to 2AP. To our knowledge, neither the two-photon action cross section for 8VA, $\eta_{VA}\delta_{VA}$, nor that for 2AP, $\eta_{AP}\delta_{AP}$, is available, but we have performed a relative measurement of the ratio of the TPA cross sections, δ_{VA}/δ_{AP}, according to the first equality in

TABLE 5: Energies and Oscillator Strengths of 8VA

method	S_1 (eV)	f_{01}	S_2 (eV)	f_{02}	θ_{mCC}, deg
TD-DFT/B3LYP/6-311+G(d,p)	4.000	0.323	4.414	0.0002	102.1
MCSCF (14,12) π-only CAS, 3A′ states	5.203	0.006	5.579	0.294	103.9
MCSCF (12,11) π-only CAS, 3A′ states	5.208		5.614		
MCQDPT2 (12,11) π-only CAS 3A′ states	4.355		4.779		
MCSCF (14,11) $2n_N$ 9π CAS, 3A′ states	5.75	0.220	5.812	0.172	83 $(S_1)^a$
MRCI (14,11) $2n_N$ 9π CAS, 3A′ states	5.382	0.180	5.465	0.210	80 $(S_2)^a$

[a] Bright.

TABLE 6: Ab Initio Electronic Dipole Moments of 8VA

method	$\|\vec{\mu}_0\|$ (D)	$\|\vec{\mu}_1\|$ (D)	$\|\vec{\mu}_2\|$ (D)	$\|\Delta\vec{\mu}_{0n}\|$ (D)	θ $(\angle\vec{\mu}_0,\vec{\mu}_n)$ (deg)
CIS/6-311+G(d,p)	3.34	1.26		4.60	178.2
MCSCF (14,12) 3 state avg. cc-pVDZ	2.98	1.53 (dark)	2.03	4.95	163.5
MRCI (14,11) 2 n, 9π cc-pVDZ	3.08	0.65 (25% H→L)^a $f_{01} = 0.18$	1.23 (36% H→L)^a $f_{02} = 0.21$	4.18	148.0
average	3.13 ± 0.19			4.58 ± 0.39	163° ± 15°

[a] H→L: HOMO→LUMO.

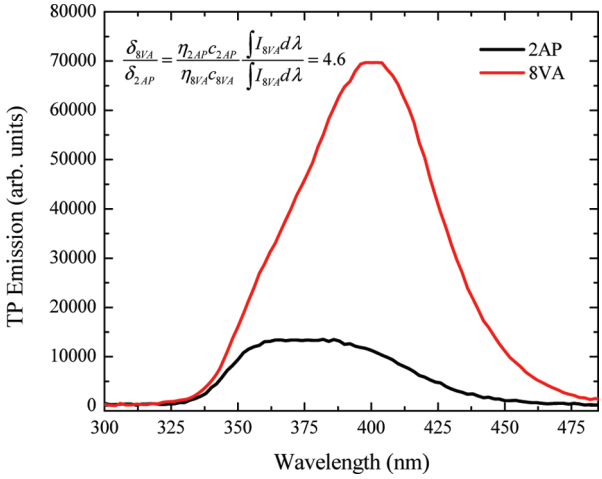

Figure 8. The fluorescence emission of 8VA (red line) and 2AP (black line) normalized for quantum yield (η), concentration, and band-pass filter transmission. The excitation wavelength was 603 nm, at the peak of 2AP monomer absorption, and within 10% of the peak absorbance of 8VA monomer.

eq 10. This can be directly compared to the calculated ratio based on eq 9 using the Stark measurements of $|\Delta\vec{\mu}_{01}^{VA}|$ and ζ_A^{VA}. We have previously measured $|\Delta\vec{\mu}_{01}^{AP}|$ and ζ_A^{AP} for 2AP by Stark spectroscopy.[44] The fluorescence quantum yields are $\eta_{VA} = 0.66$ and $\eta_{AP} = 0.68$.[33]

The two-photon-induced emission spectra of 2AP and 8VA, corrected for concentration and quantum yields and filter band-pass (see Figure 8), were integrated over the entire emission band, giving $\delta_{VA}/\delta_{AP}(TPA) = (\eta_{AP}c_{AP}/\eta_{VA}c_{VA})(\int I_{VA}\, d\nu/\int I_{AP}\, d\nu) = 4.6$. To evaluate the second equality in eq 10, we have estimated the ratio of the integrated extinction coefficients, $\int \varepsilon_{VA}\, d\nu/\int \varepsilon_{AP}\, d\nu = |\vec{m}_{01}^{VA}|^2/|\vec{m}_{01}^{AP}|^2 = 2.0$ from the absorption spectra, the ratio of the square of the difference dipole moments, $(|\Delta\vec{\mu}_{01}^{VA}|/|\Delta\vec{\mu}_{01}^{AP}|)^2 = 1.61$, and the ratio $(2\cos^2\zeta_A^{VA} + 1)/(2\cos^2\zeta_A^{AP} + 1) = 1.35$. This gives $\delta_{VA}/\delta_{AP}(Stark) = 4.4$, nearly identical with the two-photon fluorescence emission result. Both treatments predict that 8VA should have about 4.5 times the two-photon absorption cross section of 2AP.

Discussion

The room-temperature and 77 K absorption spectra and their second derivatives allowed for a deconvolution of the lowest energy bright transition with the discovery of a ca. 1460 cm^{-1} vibronic progression. This is also seen in emission with near-perfect mirror symmetry, suggesting that the ground and excited state nuclear geometries are very similar for this molecule.[67]

The Stark spectra were fitted using this absorption spectral deconvolution. To facilitate an assignment of the Stark data, we assumed that the ground state and excited state dipole moments of 8VA lie in the plane of the molecule, with the requirement that the difference dipole moment should also be in this plane. Our calculations show that the transition dipole moment is also coplanar, supporting the above simplification (an experimental determination of $\vec{m}_{01}$ is not yet available). The experimental determination that $\Delta\vec{\mu}_{01}$(4.7 D) lies at $\zeta_A = 38°$ from the transition dipole moment restricts the direction of $\Delta\vec{\mu}_{01}$ to four different possibilities. Further guidance was obtained from finite-field calculations based on TD-DFT or CIS approaches to obtain the difference dipole moment vector, $\Delta\vec{\mu}_{01}^c$ (Table 4). For TD-DFT, $\Delta\vec{\mu}_{01}^c$ is larger than the experimental value, $\Delta\vec{\mu}_{01}^{exp}$, while the CIS value is lower. The direction determined from both CIS/finite-field and TD-DFT/finite-field calculations are in good agreement with each other and agree well with only one of the four possible vectors offered from the Stark analysis. These results are further confirmed by the net difference between the excited and ground state dipole moments calculated by CIS, MCSCF, and MRCI (Table 6). Using the average of these calculated values, the "best fit" directions of $\vec{\mu}_0^c$, $\vec{\mu}_1^c$, and $\Delta\vec{\mu}_{01}^c = 4.6$ D are shown in the 8VA molecular frame (Figure 7), which agrees quite well with the Stark difference dipole moment of $\Delta\vec{\mu}_{01}^{exp} \sim 4.7$ D (after field correction). It is interesting to note that the computed ground and excited state dipole moments are nearly opposed at ~160° to each other, suggesting that significant charge redistribution occurring upon optical excitation, as confirmed by the experimental result.

Kenfack et al., using HOMO and LUMO orbitals from TD-DFT and CIS calculations,[20] obtained $|\vec{\mu}_0| = 3.11$ D based on a HF/6-31G** calculation[68] and $|\vec{\mu}_1| = 0.31$ D based on a CIS calculation using diffuse triple-ζ 6-311++G(d) basis set.[69] No value for θ $(\angle\vec{\mu}_0,\vec{\mu}_1)$ was given, but if we assume that the two static vectors are antiparallel, then $|\Delta\vec{\mu}_{01}^{VA}| = 3.42$ D, about 30% lower than our value. This prediction is quantitatively confirmed in this work both experimentally and computationally.

Kenfack et al. calculated the $S_0 \rightarrow S_1$ and $S_0 \rightarrow S_2$ transitions to lie at 291 and 264 nm with oscillator strengths of 0.250 and 0.001, respectively, at the TD-DFT/B3LYP/6-311+G(d) level of theory.[69] They suggest that the $S_0 \rightarrow S_1$ transition is a $\pi \rightarrow \pi^*$ transition and the $S_0 \rightarrow S_2$ is a $n \rightarrow \pi^*$ transition.[69] These calculations are in agreement with our calculations at the TD-DFT/B3LYP/6-311+G(d,p) level, which gave the $S_0 \rightarrow S_1$ and $S_0 \rightarrow S_2$ transitions at 310 and 280 nm with oscillator strengths of 0.320 and 0.0002, respectively. These differences could be due to different starting geometries. We optimized the 8VA geometry using the basis set given above while Kenfack et al. chose to use a geometry based on B-form DNA X-ray structures derived from INSIGHT II. The transition dipole direction calculated in this work for $S_0 \rightarrow S_1$ transition is parallel to the N_1-C_8 axis and it is consistent with the CIS calculations done by Kenfack et al.[69]

The difference in the Stokes shift between experiment[70] and theory was attributed to solvent reorganization by Kenfack et al.[68] and suggested that the smaller $\vec{\mu}_1$ for 8VA (about 0.35 D) is responsible for a lower solvent reorganization than 2AP, whose excited state dipole moment was calculated to be 4.34 D.[71] Since solvent response depends on $\Delta\vec{\mu}_{01}$, it is necessary to consider not only the magnitude of $\Delta\vec{\mu}_{01}$ but also the angle, θ, between $\vec{\mu}_0$ and $\vec{\mu}_1$. However, no vector direction was given in their work. Our experimental and computational data provided the necessary angular information to explain the smaller solvent response.

The Stark results along with the computations offer an explanation for the observed trends in solvatochromism. Our calculations suggests that $|\vec{\mu}_1| \ll |\vec{\mu}_0|$. If the dipole moment of 8VA decreases during the electronic transition, the Franck−Condon excited state is formed in a strained cage of solvent dipoles not correctly oriented for its efficient stabilization. Thus, with the increase in solvent polarity, the ground state is better stabilized, lowering its energy relative to the excited state and producing a hypsochromic shift. The superimposed bathochromic shift due to polarization will be smaller, resulting in a net hypsochromic shift.[72] This explanation is consistent with the current observation of a blue shift with increase in solvent polarity.

Another important observation from this analysis is that upon optical excitation electron density shifts from the six-membered ring to the vinyl group. This leads to a lower electron density on the amino nitrogen on C_6 and, to a smaller extent, on N_1. These groups are involved in Watson−Crick hydrogen bonds with a complementary thymine when 8VA is incorporated into dsDNA. Our results suggest that photoexcitation would lead to a weakening of the N_1 acceptor hydrogen bond but an increase in the amino donor hydrogen bond, with the potential of creating a localized transient perturbation in the hydrogen-bond network. This leads to the possibility of a "H-bond jump" experiment, similar in character to other relaxation techniques like temperature jump, where selective excitation of 8VA could induce a structural perturbation in the hydrogen-bond network in and around the excited 8VA base in double-stranded DNA or RNA. This perturbation would persist until the molecule returned to its ground state. It is possible that the magnitude of the H-bond perturbation would be sufficient to induce, for example, base flipping of the FBA or adjacent bases. This could be a valuable approach to studying DNA binding proteins, where base flipping is a part of the mechanism of action.[14,16,73] Even if the perturbation were smaller, the subsequent relaxation of the double-stranded nucleic acid could be followed using ultrafast optical spectroscopies, possibly giving site-specific information about the dynamics of double helical structure in a nucleic acid duplex that could be followed with high time resolution. This speculation however remains to be shown.

The two-photon cross sections of naturally occurring nucleic acid bases are in the range of 1−2 GM.[74] The majority of fluorescent nucleic acid base analogs currently used display $\eta\delta$ values in the range of 1−10 GM. Our Stark and computational analysis of 2AP[44] allows for an interesting comparison of the two FBAs as potential two-photon probes based on eq 9. $\Delta\vec{\mu}_{01}^{VA}$ is about 30% larger than $\Delta\vec{\mu}_{01}^{AP}$ (∼3.7 D). The orientation of $\Delta\vec{\mu}_{01}$ is also important. $\Delta\vec{\mu}_{01}^{AP}$ points toward the 2-amino group, giving $\zeta_A^{AP} = 55°$, while $\Delta\vec{\mu}_{01}^{VA}$ points away from the vinyl group with $\zeta_A^{VA} = 38°$. The ground state dipole moment points toward the 8-vinyl group, whereas the excited state dipole moment points away from the 8-vinyl group. Taken together, these facts suggest that 8VA should be significantly brighter than 2AP as a two-photon fluorophore. We have shown this to be the case by a direct measurement of the ratio of two photon-induced emission for the two analogs. The absolute value of δ still remains to be determined. When compared to 2AP, the two-photon cross section of 8VA is estimated as at least 4.5 times larger based on the information available for free base ($f_{AP} = 0.12$, $f_{VA} = 0.24$, $\Delta\vec{\mu}^{AP}{}_{01} = 3.7$D, $\Delta\vec{\mu}^{VA}{}_{01} = 4.7$D, $\zeta_A^{AP} = 55°$, $\zeta_A^{VA} = 38°$). However, no measurements of two-photon cross section of 2AP or 8VA have been reported. The TPA cross sections of a few other small molecule FBAs have been investigated. Katilius et al. studied three photon absorption by 2AP, and fluorescence correlation measurements were attempted.[75] Due to the requirements of high excitation power and long integration times, they suggested that three-photon excitation of 2AP to study the DNA base dynamics is not a viable option. However, they did measure the cross section of 2.5 GM for the pteridine-based guanine analog 6MI.[75] Our group previously measured the two photon absorption cross section of another adenine analogue 6MAP [(4-amino-6-methyl-8-(2-deoxy-β-D-ribofuranosyl)-7(8*H*)-pteridone] to be 3.4 GM at 659 nm.[76] We are in the process of evaluating the Stark parameters for these FBAs to substantiate the utility of this approach in determining TPA cross sections.

While δ is a critical quantity for TP efficiency, it is not the only consideration. The product of $\delta\eta$, where η is the fluorescence quantum yield, determines the overall brightness of the TP probe. The value of η will depend on specific interactions that the FBA undergoes with neighboring bases. In the case of 2AP, the free base fluorescence is quenched by a factor of 40 when incorporated into dsDNA (emission at 369 nm, $\eta_{monomer} = 0.68$ vs $\eta_{dsDNA} = 0.016$ in dsDNA).[18] 8VA undergoes less fluorescence quenching compared to 2AP in dsDNA. 8VA is quenched by a factor of 24[19] (emission at 382 nm, $\eta_{monomer} = 0.66$ vs $\eta_{dsDNA} = 0.028$ in dsDNA) and is therefore about 60% brighter than 2AP hybridized in dsDNA. For the purpose of two photon microscopy, we would expect that 8VA would provide an overall enhancement of $(1.6 \times 4.7) = 7.5$ in signal level over 2AP, a significant improvement. Another interesting observation made by Gaied et al. is that 8VA is relatively less quenched in double-stranded DNA compared to single-stranded DNA, whereas this is the opposite case for 2AP,[18] opening the possibility for studying ssDNA dynamics with even higher signal-to-noise.

In the end, however, the optical emission, absorption, and Stark measurements and ab initio calculations do not shed light on the nature of the emitting electronic states in 8VA compared to 2AP.[77] In the case of the latter, Perun et al. have suggested that the emitting state quantum yield of 2AP relative to adenine

represents a competition between radiative decay and nonradiative decay via a conical intersection achieved when adenine undergoes a twisting deformation about the CN bond of the six-membered ring. Matsika's group has shown the importance of these conical intersections in the low quantum yield of the native bases.[78,79] The current results show that 8VA has an advantage over 2AP for the absorption event, but the increased emission yield appears to involve the emitting state well outside the Franck−Condon region. Calculations need to be done to ascertain whether there is a high activation barrier for excited 8VA to reach a conical intersection and to what extent base stacking in dsDNA stabilizes the emitting state by disallowing the molecule from distorting to the geometry necessary to arrive at the intersection. From an experimental perspective, it will be illuminating to gather data on the excited state electronic properties of 8VA in a duplex using the methods described here, especially Stark fluorescence spectroscopy,[80−83] where the nature of the emitting state can be explored in great detail.

Conclusions

We have measured the change in electronic structure for 8VA for its lowest energy optically bright transition using Stark spectroscopy. The experimental results were supplemented with an ab initio study of the molecule, which showed that intramolecular charge transfer moves electron density away from the purine ring and onto the vinyl group. This charge redistribution provides for a significant difference dipole vector, whose direction is less than 40° from the transition dipole moment vector. These attributes suggest that 8VA may have a significant TPA cross section. Indeed, a measurement of the ratio of TP emission intensities for 8VA vs 2AP shows that 8VA fluorescence is nearly 5 times brighter than 2AP. On the basis of this study, the superiority of 8VA as a two-photon probe must be ascribed to an increased oscillator strength, the increased $\Delta\bar{\mu}_{01}$, *and* the lower value of ζ_A, all of which contribute to a large degree of intramolecular charge transfer. The ability to measure these quantities accurately with Stark spectroscopy, a technique that uses steady-state light sources and modest electronics, points to its use as a routine method of screening for TPA molecular probes.

Acknowledgment. The authors wish to thank Murali V.V.N.D and Dr. Rodrigo Andrade for help in synthesizing the 8VA and for providing lab space and resources. We are also grateful to Mr. Oleksandr Isaienko and Dr. Eric Borguet for the use of their regenerative amplifier. G.K. and R.J.S. are grateful for support from the NSF Molecular Biosciences Division (MCB-0347087) and for a Temple University Bridge Grant. S.M. acknowledges support from NSF (CHE-0449853 and CHE-0911474). K.A.K. is partially supported by a Case Fellowship (Department of Chemistry, Temple University). This research was supported in part by grant number MCB080057P from the Pittsburgh Supercomputing Center, supported by several federal agencies, the Commonwealth of Pennsylvania, and private industry.

Supporting Information Available: Figures as discussed in the text. This material is available free of charge via the Internet at http://pubs.acs.org.

References and Notes

(1) Tinsley, R. A.; Walter, N. G. *RNA* **2006**, *12*, 522.
(2) Bloom, L. B.; Otto, M. R.; Beechem, J. M.; Goodman, M. F. *Biochemistry* **1993**, *32*, 11247.
(3) Frey, M. W.; Sowers, L. C.; Millar, D. P.; Benkovic, S. J. *Biochemistry* **1995**, *34*, 9185.
(4) Turingan, R. S.; Liu, C. H.; Hawkins, M. E.; Martin, C. T. *Biochemistry* **2007**, *46*, 1714.
(5) Raney, K. D.; Sowers, L. C.; Millar, D. P.; Benkovic, S. J. *Proc. Natl. Acad. Sci. U.S.A.* **1994**, *91*, 6644.
(6) Holz, B.; Klimasauskas, S.; Serva, S.; Weinhold, E. *Nucleic Acids Res.* **1998**, *26*, 1076.
(7) Allan, B. W.; Beechem, J. M.; Lindstrom, W. M.; Reich, N. O. *J. Biol. Chem.* **1998**, *273*, 2368.
(8) Allan, B. W.; Reich, N. O. *Biochemistry* **1996**, *35*, 14757.
(9) Zang, H.; Fang, Q.; Pegg, A. E.; Guengerich, F. P. *J. Biol. Chem.* **2005**, *280*, 30873.
(10) McCullough, A. K.; Dodson, M. L.; Scharer, O. D.; Lloyd, R. S. *J. Biol. Chem.* **1997**, *272*, 27210.
(11) Nordlund, T. M.; Andersson, S.; Nilsson, L.; Rigler, R.; Graeslund, A.; McLaughlin, L. W. *Biochemistry* **1989**, *28*, 9095.
(12) Rachofsky, E. L.; Seibert, E.; Stivers, J. T.; Osman, R.; Ross, J. B. A. *Biochemistry* **2001**, *40*, 957.
(13) Stivers, J. T.; Pankiewicz, K. W.; Watanabe, K. A. *Biochemistry* **1999**, *38*, 952.
(14) Christine, K. S.; MacFarlane, A. W., IV; Yang, K.; Stanley, R. J. *J. Biol. Chem.* **2002**, *277*, 38339.
(15) Yang, K.; Stanley, R. J. *Biochemistry* **2006**, *45*, 11239.
(16) Yang, K.; Matsika, S.; Stanley, R. J. *J. Phys. Chem., B* **2007**, *111*, 10615.
(17) Yang, K.; Stanley, R. J. *Photochem. Photobiol.* **2008**, *84*, 741.
(18) Gaied, N. B.; Glasser, N.; Ramalanjaona, N.; Beltz, H.; Wolff, P.; Marquet, R.; Burger, A.; Me'ly, Y. *Nucleic Acids Res.* **2005**, *33*, 1031.
(19) Kenfack, C. A.; Piemont, E.; Ben Gaied, N.; Burger, A.; Mely, Y. *J. Phys. Chem. B* **2008**, *112*, 9736.
(20) Kenfack, C. A.; Burger, A.; Mely, Y. *J. Phys. Chem. B* **2006**, *110*, 26327.
(21) Roday, S.; Saen-oon, S.; Schramm, V. L. *Biochemistry* **2007**, *46*, 6169.
(22) Jean, J. M.; Hall, K. B. *Proc. Natl. Acad. Sci. U.S.A.* **2001**, *98*, 37.
(23) Jean, J. M.; Hall, K. B. *J. Phys. Chem. A* **2000**, *104*, 1930.
(24) Jean, J. M.; Hall, K. B. *Biochemistry* **2002**, *41*, 13152.
(25) Rachofsky, E. L.; Osman, R.; Ross, J. B. *Biochemistry* **2001**, *40*, 946.
(26) Hawkins, M. E.; Pfleiderer, W.; Jungmann, O.; Balis, F. M. *Anal. Biochem.* **2001**, *298*, 231.
(27) Evans, K.; Xu, D.; Kim, Y.; Nordlund, T. M. *J. Fluoresc.* **1992**, *2*, 209.
(28) Jean, J. M.; Hall, K. B. *Biochemistry* **2004**, *43*, 10277.
(29) Larsen, O. F. A.; Van Stokkum, I. H. M.; Gobets, B.; Van Grondelle, R.; Van Amerongen, H. *Biophys. J.* **2001**, *81*, 1115.
(30) Fiebig, T.; Wan, C.; Zewail, A. H. *ChemPhysChem* **2002**, *3*, 781.
(31) O'Neill, M. A.; Becker, H.-C.; Wan, C.; Barton, J. K.; Zewail, A. H. *Angew. Chem., Int. Ed.* **2003**, *42*, 5896.
(32) Wan, C.; Fiebig, T.; Schiemann, O.; Barton, J. K.; Zewail, A. H. *Proc. Natl. Acad. Sci. U.S.A.* **2000**, *97*, 14052.
(33) Ward, D. C.; Reich, E.; Stryer, L. *J. Biol. Chem.* **1969**, *244*, 1228.
(34) Bierzynski, A.; Kozlowska, H.; Wierzchowski, K. I. *Biophys. Chem.* **1977**, *6*, 223.
(35) Boxer, S. G. *J. Phys. Chem. B* **2009**, *113*, 2972.
(36) Nakagawa, K.; Suzuki, S.; Fujii, R.; Gardiner, A. T.; Cogdell, R. J.; Nango, M.; Hashimoto, H. *Photosynth. Res.* **2008**, *95*, 339.
(37) Somsen, O. J. G.; Chernyak, V.; Frese, R. N.; Van Grondelle, R.; Mukamel, S. *J. Phys. Chem. B* **1998**, *102*, 8893.
(38) Mathies, R.; Stryer, L. *Proc. Natl. Acad. Sci. U.S.A.* **1976**, *73*, 2169.
(39) Kodali, G.; Siddiqui, S. U.; Stanley, R. J. *J. Am. Chem. Soc.* **2009**, *131*, 4795.
(40) Chowdhury, A.; Locknar, S. A.; Premvardhan, L. L.; Peteanu, L. A. *J. Phys. Chem. A* **1999**, *103*, 9614.
(41) Karki, L.; Vance, F. W.; Hupp, J. T.; LeCours, S. M.; Therien, M. J. *J. Am. Chem. Soc.* **1998**, *120*, 2606.
(42) Bublitz, G. U.; Ortiz, R.; Marder, S. R.; Boxer, S. G. *J. Am. Chem. Soc.* **1997**, *119*, 3365.
(43) Liptay, W. Dipole Moments and Polarizabilities of Molecules in Excited Electronic States. In *Excited States*; Lim, E. C., Ed.; Academic Press, Inc.: New York, 1974; Vol. 1; pp 129.
(44) Kodali, G.; Kistler, K. A.; Matsika, S.; Stanley, R. J. *J. Phys. Chem. B* **2008**, *112*, 1789.
(45) Van Aerschot, A. A.; Mamos, P.; Weyns, N. J.; Ikeda, S.; De Clercq, E.; Herdewijn, P. A. *J. Med. Chem.* **1993**, *36*, 2938.
(46) Kodali, G.; Kistler, K. A.; Matsika, S.; Stanley, R. J. *J. Phys. Chem. B* **2008**, *112*, 1789.
(47) Stanley, R. J.; Siddiqui, M. S. *J. Phys. Chem. A* **2001**, *105*, 11001.
(48) Bublitz, G. U.; Boxer, S. G. *Annu. Rev. Phys. Chem.* **1997**, *48*, 213.
(49) Albrecht, C. *Principles of Fluorescence Spectroscopy*, 3rd ed., Lakowicz, J. R., Ed.; 2008; Vol. 390.

(50) Kawski, A. *Z. Naturforsch., A: Phys. Sci.* **2002**, *57*, 255.
(51) Bakhshiev, N. G.; Knyazhanskii, M. I.; Minkin, V. I.; Osipov, O. A.; Saidov, G. V. *Usp. Khim.* **1969**, *38*, 1644.
(52) Jedrzejewska, B.; Kabatc, J.; Osmialowski, B.; Paczkowski, J. *Spectrochim. Acta, Part A* **2007**, *67A*, 306.
(53) Bilot, L.; Kawski, A. *Z. Naturforsch.* **1962**, *17a*, 621.
(54) Isaienko, O.; Borguet, E. *J. Opt. Soc. Am. B* **2009**, *26*, 965.
(55) Day, P. N.; Nguyen, K. A.; Pachter, R. *J. Phys. Chem. B* **2005**, *109*, 1803.
(56) Schmidt, M. W.; Baldridge, K. K.; Boatz, J. A.; Elbert, S. T.; Gordon, M. S.; Jensen, J. J.; Koseki, S.; Matsunaga, N.; Nguyen, K. A.; Su, S.; Windus, T. L.; Dupuis, M.; Montgomery, J. A. *J. Comput. Chem.* **1993**, *14*, 1347.
(57) Lischka, H.; Shepard, R.; Shavitt, I.; Pitzer, R. M.; Dallos, M.; Müller, T.; Szalay, P. G.; Brown, F. B.; Ahlrichs, R.; Böhm, H. J.; Chang, A.; Comeau, D. C.; Gdanitz, R.; Dachsel, H.; Ehrhardt, C.; Ernzerhof, M.; Höchtl, P.; Irle, S.; Kedziora, G.; Kovar, T.; Parasuk, V.; Pepper, M. J. M.; Scharf, P.; Schiffer, H.; Schindler, M.; Schüler, M.; Seth, M.; Stahlberg, E. A.; Zhao, J.-G.; Yabushita, S.; Zhang, Z. *COLUMBUS, an Ab Initio Electronic Structure Program, Release 5.8*, 2001.
(58) Lischka, H.; Shepard, R.; Pitzer, R. M.; Shavitt, I.; Dallos, M.; Müller, T.; Szalay, P. G.; Seth, M.; Kedziora, G. S.; Yabushita, S.; Zhang, Z. *Phys. Chem. Chem. Phys.* **2001**, *3*, 664.
(59) Lischka, H.; Shepard, R.; Brown, F. B.; Shavitt, I. *Int. J. Quantum Chem.: Quantum Chem. Symp.* **1981**, *15*, 91.
(60) Frisch, M. J.; Trucks, G. W.; Schlegel, H. B.; Scuseria, G. E.; Robb, M. A.; Cheeseman, J. R. J. AMontgomery, J.; T. Vreven, K. N. K.; J. C. Burant, J. M. M.; Iyengar, S. S.; Tomasi, J.; Barone, V.; Mennucci, B.; Cossi, M.; Scalmani, G.; Rega, N.; Petersson, G. A.; Nakatsuji, H.; Hada, M.; Ehara, M.; Toyota, K.; Fukuda, R.; Hasegawa, J.; Ishida, M.; Nakajima, T.; Honda, Y.; Kitao, O.; Nakai, H.; Klene, M.; Li, X.; Knox, J. E.; Hratchian, H. P.; Cross, J. B.; Adamo, C.; Jaramillo, J.; Gomperts, R.; Stratmann, R. E.; Yazyev, O.; Austin, A. J.; Cammi, R.; Pomelli, C.; Ochterski, J. W.; Ayala, P. Y.; Morokuma, K.; Voth, G. A.; Salvador, P.; Dannenberg, J. J.; Zakrzewski, V. G.; Dapprich, S.; Daniels, A. D.; Strain, M. C.; Farkas, O.; Malick, D. K.; Rabuck, A. D.; Raghavachari, K.; Foresman, J. B.; Ortiz, J. V.; Cui, Q.; Baboul, A. G.; Clifford, S.; Cioslowski, J.; Stefanov, B. B.; Liu, G.; Liashenko, A.; Piskorz, P.; Komaromi, I.; Martin, R. L.; Fox, D. J.; Keith, T.; Al-Laham, M. A.; Peng, C. Y.; Nanayakkara, A.; Challacombe, M.; Gill, P. M. W.; Johnson, B.; Chen, W.; Wong, M. W.; Gonzalez, C.; Pople, J. A. *Gaussian 07, Revision A*; Gaussian, Inc.: Pittsburgh, PA, 2003.
(61) Dunning, T. H. *J. Chem. Phys.* **1989**, *90*, 1007.
(62) Kistler, K. A.; Matsika, S. *J. Phys. Chem. A* **2007**, *111*, 8708.
(63) Cances, E.; Mennucci, B.; Tomasi, J. *J. Chem. Phys.* **1997**, *107*, 3032.
(64) Mennucci, B.; Tomasi, J. *J. Chem. Phys.* **1997**, *106*, 5151.
(65) Dreuw, A.; Head-Gordon, M. *Chem. Rev. (Washington, DC)* **2005**, *105*, 4009.
(66) Mburu, E.; Matsika, S. *J. Phys. Chem. A* **2008**, *112*, 12485.
(67) Gurinovich, G. P.; Sevchenko, A. N.; Solov'ev, K. N. *Usp. Fiz Nauk* **1963**, *79*, 173.
(68) Kenfack, C. A.; Piemont, E.; Ben Gaied, N.; Burger, A.; Mély, Y. *J. Phys. Chem. B* **2008**, *112*, 9736.
(69) Kenfack, C. A.; Burger, A.; Mély, Y. *J. Phys. Chem. B* **2006**, *110*, 26327.
(70) Ben Gaied, N.; Glasser, N.; Ramalanjaona, N.; Beltz, H.; Wolff, P.; Marquet, R.; Burger, A.; Mély, Y. *Nucleic Acids Res.* **2005**, *33*, 1031.
(71) Jean, J. M.; Hall, K. B. *J. Phys. Chem. A* **2000**, *104*, 1930.
(72) Reichardt, C. *Solvents and Solvent Effects in Organic Chemistry*; VCH Verlagsgesellschaft mbH: Weinheim, 1988.
(73) Roberts, R. J. *Cell* **1995**, *82* (1), 9.
(74) Yu P Meshalkin, E. E. A.; Makukha, V. K. *Quant. Electron.* **1998**, *28*, 725.
(75) Katilius, E.; Woodbury, N. W. *J. Biomed. Opt.* **2006**, *11*, 044004/1.
(76) Stanley, R. J.; Hou, Z.; Yang, A.; Hawkins, M. E. *J. Phys. Chem. B* **2005**, *109*, 3690.
(77) Perun, S.; Sobolewski, A. L.; Domcke, W. *Mol. Phys.* **2006**, *104*, 1113.
(78) Kistler, K. A.; Matsika, S. *J. Phys. Chem. A* **2007**, *111*, 2650.
(79) Matsika, S. *J. Phys. Chem. A* **2004**, *108*, 7584.
(80) Lockhart, D. J.; Boxer, S. G. *Chem. Phys. Lett.* **1988**, *144*, 243.
(81) Lockhart, D. J.; Goldstein, R. F.; Boxer, S. G. *J. Chem. Phys.* **1988**, *89*, 1408.
(82) Smith, T. M.; Hazelton, N.; Peteanu, L. A.; Wildeman, J. *J. Phys. Chem. B* **2006**, *110*, 7732.
(83) Ohta, N.; Umeuchi, S.; Nishimura, Y.; Yamazaki, I. *J. Phys. Chem. B* **1998**, *102*, 3784.

JP908055H